

# Mars Entry Bank Profile Design for Terminal State Optimization

Jarret M. Lafleur\* and Chris J. Cerimele†  
 NASA Johnson Space Center, Houston, Texas 77058

One challenge examined in NASA's DRM 5.0 study is that of entry, descent, and landing (EDL) on Mars for high-ballistic-coefficient, human-class payloads. To define best-case entry scenarios for the evaluation of potential EDL system designs, a study is conducted to optimize the entry-to-terminal-state portion of EDL for a variety of entry velocities, vehicle ballistic coefficients ( $\beta$ ), and lift-to-drag ratios ( $L/D$ ). The terminal state is envisioned as one appropriate for the initiation of terminal descent via parachute or other means. A particle swarm optimizer varies entry flight path angle and ten bank profile points to find maximum-final-altitude trajectories. A baseline set of optimizations is performed, as are full-lift-up and relaxed-deceleration-constraint sets for comparison. In total, an estimated 9 million trajectories are analyzed to yield 1800 optimal trajectories. Parametric plots of maximum achievable altitude are shown, as are examples of optimized trajectories. Characteristic vehicle contours are overlaid on the parametric plots, and conclusions are drawn on the feasibility of vehicles in the  $L/D$  vs.  $\beta$  design space. It is shown that entry bank angle control is highly deserving of consideration early in design, particularly for vehicles with mid- or high- $L/D$  values, high entry velocities, and deceleration-limited trajectories. Key conclusions are also drawn regarding trends in optimal bank profiles and in the constraints which impose particularly severe limits on the design of these trajectories.

## Nomenclature

$a$	= vehicle acceleration	$L/D$	= vehicle hypersonic lift-to-drag ratio
$C_D$	= vehicle drag coefficient	$m$	= vehicle mass
$C_L$	= vehicle lift coefficient	$MOLA$	= Mars Orbiter Laser Altimeter
$D$	= drag force on vehicle	$MSL$	= Mars Science Laboratory
$d$	= drag direction unit vector	$NASA$	= National Aeronautics and Space Administration
$DRM$	= Design Reference Mission	$q$	= dynamic pressure
$EDL$	= Entry, Descent, and Landing	$r$	= vector from planet center to vehicle mass center
$g$	= local gravitational acceleration	$S$	= vehicle reference area
$h$	= altitude above reference ellipsoid	$v_{rel}$	= vehicle velocity relative to surface of planet
$L$	= lift force on vehicle	$\beta$	= vehicle ballistic coefficient
$l$	= lift direction unit vector	$\rho$	= local atmospheric density

## I. Introduction

IN January 2007, NASA assembled an agency-wide team of scientists and engineers to develop a current assessment of objectives, system requirements, and prerequisites for human Mars exploration. As a collaborative effort among all four mission directorates, the objectives of the study were to (1) update NASA's human Mars mission reference architecture as DRM 5.0, (2) develop a plan of research and technology investments to reduce human Mars mission cost and risk, and (3) assess strategic linkages between human lunar and Mars exploration.

One key challenge under examination as part of DRM 5.0 was that of conducting entry, descent, and landing for human-class payloads. Coupling these massive payloads with launch-vehicle-limited aeroshell diameters typically

\*Graduate Co-op Student, Flight Mechanics and Trajectory Design Branch/EG5, Student Member AIAA.

†Branch Chief, Flight Mechanics and Trajectory Design Branch/EG5, Member AIAA.

results in very high vehicle ballistic coefficients and low  $L/D$  which, for Mars, results in very supersonic terminal velocities. It is generally impossible to decelerate these vehicles to velocities much lower than Mach 1.5 or Mach 2 without the assistance of supersonic propulsion, large supersonic parachutes, or other large inflatable aerodynamic decelerators, none of which are yet proven for the Martian environment.

To define best-case entry scenarios for the evaluation of potential descent and landing system designs, this paper focuses on the optimization of the entry-to-terminal-state phase for a variety of entry velocities, vehicle ballistic coefficients, and lift-to-drag ratios by selecting appropriate entry flight path angles and bank angle profiles. The terminal state is envisioned as one appropriate for initiation of a terminal descent system, such as a parachute. As is shown at the conclusion of this paper, this study permits identification of optimal regions of the ballistic-coefficient-versus- $L/D$  design space for any given entry vehicle capability envelope, which is important for minimizing the performance demands (and, in turn, technology demands) on terminal descent systems. From the perspective of the aerodynamic decelerator, parachute, or propulsion designer, this study effectively black-boxes the entry phase of flight for a best-case entry for a variety of vehicle configurations and entry conditions. As will soon be discussed, the metric chosen to represent these “best” cases is the maximum achievable altitude at a given Mach number.

### A. Previous Work on Entry Bank Profile Design

Design of bank angle modulation profiles to control flight in the hypersonic regime of atmospheric entry is well-established. Banking during atmospheric entry allows for the rotation of a vehicle’s lift vector (see Fig. 1) and thus allows a degree of control for achieving target landing sites or other trajectory objectives. A variety of guidance algorithms have been developed to effect these bank angle modulations, and entry guidance has been employed in Earth entry for manned vehicles since the Gemini program. However, only recently has guidance been developed for precision landing on Mars.

One of the most noteworthy applications of bank angle control for Mars is in the Mars Science Laboratory (MSL) mission slated to fly in 2009. MSL uses a modified Apollo guidance algorithm requiring the definition of a reference bank profile. Unlike the manned Apollo missions, which used a constant-bank reference profile, MSL utilizes a variable-bank profile which is divided into three segments in the relative velocity domain. The use of this variable-bank profile is necessitated by the inability of a constant-bank profile to meet parachute deployment constraints (e.g. altitude and dynamic pressure).<sup>1</sup> Extensive work has been performed to design this three-segment reference bank profile for the approximately 140 kg/m<sup>2</sup> ballistic coefficient, 0.24 lift-to-drag-ratio vehicle.

However, to date, no study known to the authors has considered the systematic optimization of high-ballistic-coefficient Mars entry trajectories through control of bank angle profile. Some past studies have made broad parametric sweeps, as this study does, but have assumed a full-lift-up profile throughout the trajectory.<sup>2,3</sup> While intuition may suggest that a full-lift-up trajectory is most advantageous in terms of final altitude, often a lift-down bank angle early during entry allows a vehicle to dive and spend more time in high-drag (and high-lift) regions lower in the atmosphere. Other studies, such as for MSL, consider bank angle optimization but only for specific cases with relatively low ballistic coefficients.<sup>4</sup> Substantial gains are possible through control of the lift vector, and it is prudent to consider the performance effects of banking in any parametric assessment of Mars vehicle designs. This is especially true for the high-ballistic-coefficient, and likely high-lift-to-drag ratio, human-class vehicles toward which this study is directed.

### B. Challenges in the Physics of Mars Entry

Entry, descent, and landing on Mars is particularly challenging because of the physical characteristics of Mars itself. Unlike Earth, which has a relatively thick atmosphere and high gravity, and the Moon, which has no atmosphere but low gravity, Mars has essentially the worst of both worlds: a thin atmosphere and relatively high gravity. As an illustration of Mars’ aerodynamic “unfriendliness”, a previous study<sup>5</sup> has shown that heavier-than-air flight on Mars requires 2.1 times as much power as on Earth and 17.5 times as much power as on Titan due to the high value of  $g^{1.5}/\rho^{0.5}$  on Mars.

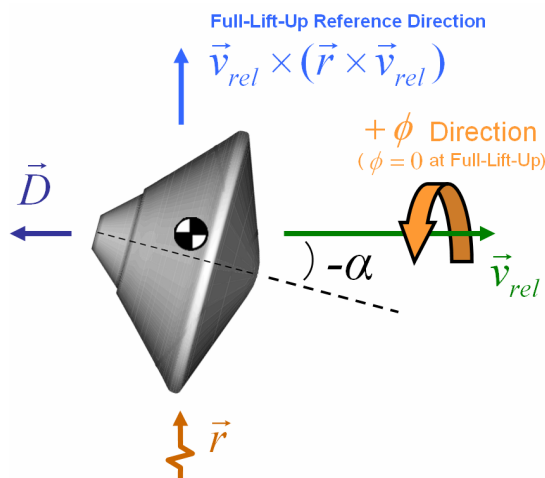


Figure 1. Bank angle ( $\phi$ ) definition.

Another illustration of Mars' aerodynamic unfriendliness is shown in Fig. 2, which plots terminal velocity on Mars as a function of altitude above the MOLA reference ellipsoid ( $h$ ) and vehicle ballistic coefficient ( $\beta$ ). As shown in Eq. (1), terminal velocity is a function only of ballistic coefficient, local gravitational acceleration, and local atmospheric density (the latter two of which are functions of altitude). The definition of ballistic coefficient is shown in Eq. (2) (note that  $m$  is object mass,  $C_D$  is object drag coefficient, and  $S$  is object reference area).

Note from Fig. 2 that terminal Mach number on Mars is generally about a factor of ten higher on Mars than for the same ballistic coefficient and altitude on Earth. This highlights the extreme challenge that Mars poses in terms of entry, descent, and landing: Any vehicle with a ballistic coefficient greater than  $85 \text{ kg/m}^2$  would naturally impact the Martian surface supersonically. This is in stark contrast to Earth, where an  $85 \text{ kg/m}^2$  vehicle would impact the ground at about Mach 0.10. As a further illustration, based on data available from Ref. 6, it can be estimated that a skydiver on Mars would have a terminal velocity somewhere in the range of Mach 1.0 to 1.5 (assuming a ballistic coefficient of between  $90$  and  $180 \text{ kg/m}^2$ , depending on the degree of the transonic drag rise).

A final note to make on Fig. 2 is that later in this paper, it will be seen that many optimal trajectories are able to reach some altitudes at velocities lower than the terminal velocity at that altitude. For example, one optimal trajectory yields a vehicle which reaches Mach 2 at  $6.8 \text{ km}$  for a  $600 \text{ kg/m}^2$  vehicle even though terminal velocity at  $6.8 \text{ km}$  for a  $600 \text{ kg/m}^2$  ballistic coefficient is Mach 3.6. The reason this sub-terminal velocity is possible is because of the presence of lift, which provides the vehicle with some authority to loft and thereby trade kinetic energy (i.e. velocity) for potential energy (i.e. altitude).

$$V_{term} = \sqrt{2\beta \frac{g}{\rho}} \quad (1)$$

$$\beta = \frac{m}{C_D S} \quad (2)$$

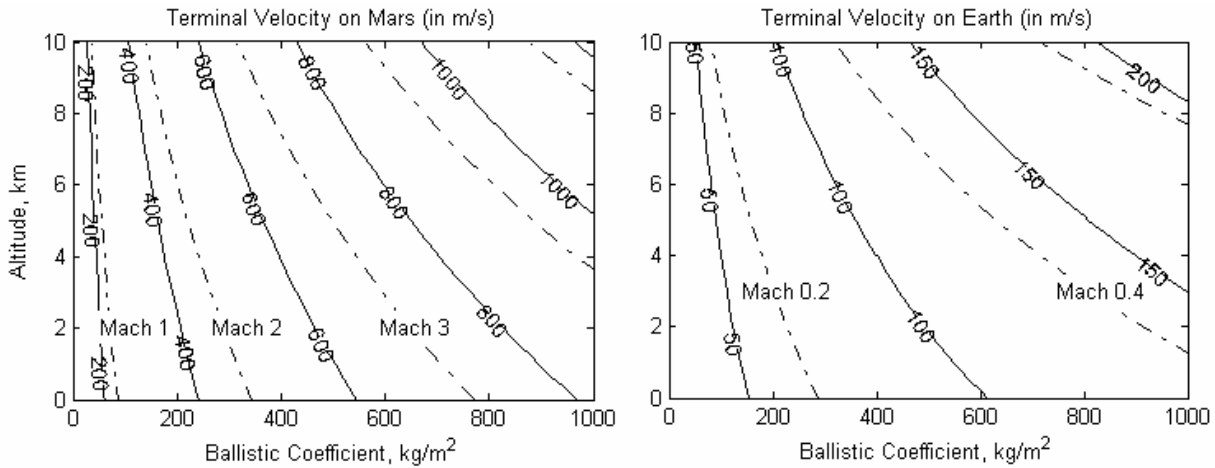


**Figure 2. Terminal velocities (in m/s) and Mach numbers on Mars (left) and Earth (right) as a function of altitude and ballistic coefficient.**

### C. Vehicle Parameterization

One principle on which this study relies is that a given entry vehicle can, from a trajectory perspective, be completely described by ballistic coefficient ( $\beta$ ) and lift-to-drag ratio ( $L/D$ ). This principle hinges on the assumption of a constant trim drag coefficient ( $C_D$ ) and  $L/D$ , which is approximately true for hypersonic flight. A proof of the validity of this parameterization is shown below:

Beginning with the definition of ballistic coefficient given in Equation 2, the definition of  $L/D = C_L/C_D$ , and Newton's second law for a constant-mass object, a vector equation of motion may be derived. For entry, the only forces acting on a vehicle are lift ( $L$ ), drag ( $D$ ), and gravity ( $mg$ ), allowing the force term to be

written as in Eq. (3) below, where hat (^) terms indicate unit vectors in the respective directions of lift and drag. Equation (4) is equivalent to Eq. (3) except with all terms normalized by  $m$ . Note that  $q$  is dynamic pressure.

$$\vec{F} = \vec{L} + \vec{D} + m\vec{g} = qSC_L\hat{l} + qSC_D\hat{d} + m\vec{g} \quad (3)$$

$$\frac{\vec{F}}{m} = \frac{qS}{m}(C_L\hat{l} + C_D\hat{d}) + \vec{g} = \frac{qSC_D}{m}\left(\frac{C_L}{C_D}\hat{l} + \hat{d}\right) + \vec{g} \quad (4)$$

Recognizing that  $SC_D/m = 1/\beta$  and that  $C_L/C_D = L/D$ , Eq. (4) can be written as:

$$\frac{\vec{F}}{m} = \frac{q}{\beta}\left(\frac{L}{D}\hat{l} + \hat{d}\right) + \vec{g} \quad (5)$$

Expressing the  $l$  and  $d$  unit vectors in physical terms and recognizing that the left hand side is actually the vehicle's acceleration allows Eq. (5) to be written in its final form as:

$$\vec{a} = \frac{q}{\beta}\left(\frac{L}{D} \cdot (\hat{v}_{rel} \times (\hat{r} \times \hat{v}_{rel})) - \hat{v}_{rel}\right) + \vec{g} \quad (6)$$

Note that in Eq. (6), the vehicle's acceleration (the highest-order state derivative) is a function only of the vehicle's current state ( $q$  is a function only of velocity and density, which is a function of altitude, and  $g$  is a function only of altitude) and the parameters  $\beta$  and  $L/D$ . As long as  $\beta$  and  $L/D$  are assumed constants (as is approximately true for trimmed hypersonic conditions), then this equation shows that the entry dynamics of a vehicle on a given planet can be completely described by  $\beta$  and  $L/D$ .

Ballistic coefficients and  $L/D$  values for several historical and future entry vehicles are shown in Table 1 and Table 2. Note that all robotic Mars entries flown to date have utilized either zero-lift ballistic trajectories or full-lift-up profiles, which has primarily been acceptable to the terminal descent system design because of their low ballistic coefficients. The Mars Science Laboratory mission, however, utilizes banking, and all U.S. manned vehicles since Gemini have also utilized banking. The manned vehicles are particularly relevant to the context of this study because they illustrate the high ballistic coefficients typically associated with manned flight.

**Table 1. Entry Characteristics of Selected Mars Landers.**<sup>7-11</sup>

Vehicle	Viking 1	Pathfinder	Mars Microprobes	Beagle 2	MER-A	Phoenix	MSL
Last Entry Date	1976	1997	1999	2003	2004	2008	2010*
Entry $\beta$ (kg/m <sup>2</sup> )	64	63	36	73	94	65	140
Hypersonic L/D	0.18	0	0	0	0	0	0.24
Bank Scheme	Full Lift-Up	N/A	N/A	N/A	N/A	N/A	Guided

\*Expected

**Table 2. Entry Characteristics of Selected Manned Vehicles.**<sup>12-18</sup>

Vehicle	Mercury	Vostok	Gemini	Apollo	X-38	Soyuz	Space Shuttle
Last Entry Date	1963	1963	1966	1975	N/A	2008**	2008**
Entry $\beta$ (kg/m <sup>2</sup> )	260	580	330	380	920	590	530
Hypersonic L/D	0	0	0.17	0.32	0.92	0.28	1.4
Bank Scheme	N/A	N/A	Guided	Guided	Guided	Guided	Guided

\*\*As of writing of this paper; flights are ongoing.

## II. Assumptions and Objective Function Selection

### A. Objective Function

One of the first steps in this study is the definition of an objective function by which to define an “optimal” trajectory. If a vehicle is defined and sizing models are available, the most obvious choice is the maximization of landed payload mass for a given entry mass or, equivalently, the minimization of entry mass for a given landed payload mass. However, in this study, an entry vehicle is not defined beyond  $L/D$  and ballistic coefficient.

Instead of vehicle mass minimization, this study seeks altitude maximization for a given trajectory termination Mach number. The inherent assumption behind this objective is that it is desirable for an entry vehicle to be traveling as slow and as high as possible when terminal descent is initiated (via parachutes, inflatable aerodynamic decelerators, or propulsion). The reason for this is rooted in altitude being a proxy for time-to-ground. To help explain this, Fig. 3 shows the variation of potential and kinetic energy with time for a vehicle entering at 4.7 km/s with  $\beta = 200 \text{ kg/m}^2$  and  $L/D = 0.5$  on a maximum-altitude trajectory terminating at Mach 2. Note that the potential energy associated with altitude is a small fraction of the total energy, even at the end of the trajectory. Furthermore, potential energy changes relatively little even with large changes in altitude. Thus, while entry may be considered a total energy minimization problem (on the trajectory below, 98.3% of vehicle total energy is removed by Mach 2), kinetic energy changes are of principal importance. High altitude is known to be an important indicator of time available during parachute or inflatable device phases, and it also indicates the ease with which low-altitude terminal states may be achieved. Thus, since high altitude is also not a significant player in terms of energy, it is used as a defining characteristic of optimum trajectories.

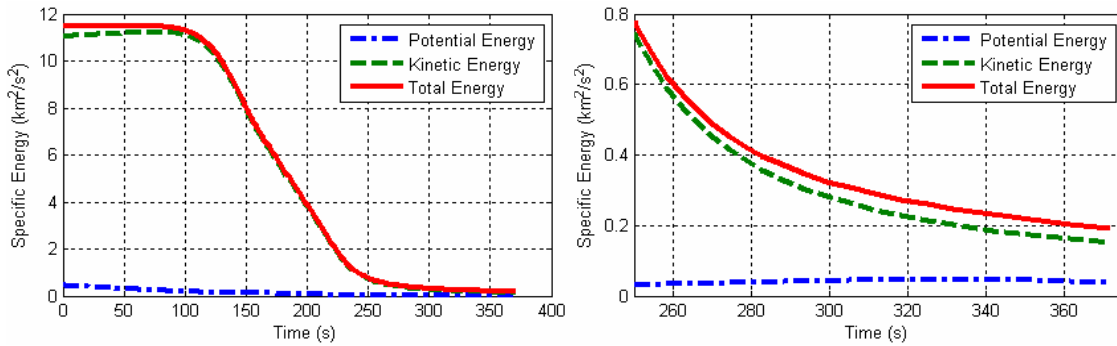


**Figure 3. Specific energy for a  $\beta = 200 \text{ kg/m}^2$ ,  $L/D = 0.5$  vehicle entering at 4.7 km/s on a maximum-altitude trajectory terminating at Mach 2. The right graph magnifies the final 2 minutes of flight.**

### B. Assumptions

In the completion of this study, several assumptions are made. The most significant is the assumption of an atmosphere. For consistency purposes with corresponding human Mars entry simulation efforts at other NASA centers, an equatorial landing site is assumed for entry on November 3, 2010 (Julian date 2455503.5). The corresponding atmospheric density and temperature profiles from the widely-used Mars-GRAM engineering-level atmospheric model<sup>19</sup> are shown in Fig. 4. Altitudes reported are above the MOLA reference ellipsoid.

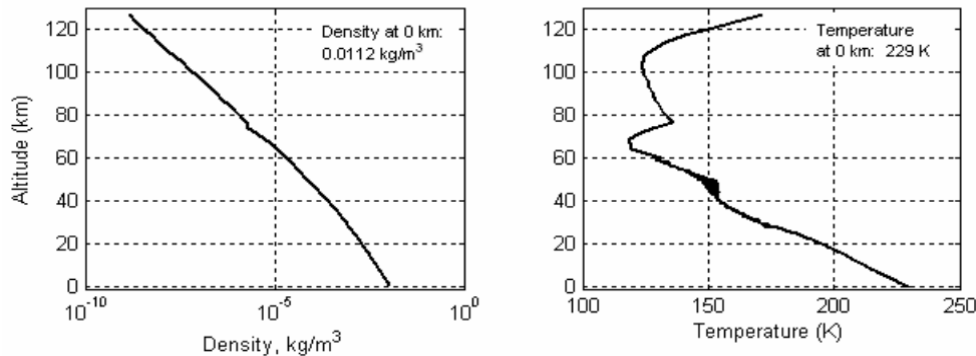


**Figure 4. Density and Temperature profiles for the atmosphere assumed for this study.**

As described earlier, a constant-trim condition is assumed for hypersonic flight, and as a result, a vehicle can be completely defined by a ballistic coefficient and lift-to-drag ratio. Additionally, this study assumes a 10-point bank profile defined in terms of points evenly spaced in the relative velocity domain. Bank angle is linearly interpolated between each of these points, much as was done by Ref. 4.

Constraints include a 4.5 Earth-G acceleration limit to reflect acceptable deceleration for a deconditioned human crew while also allowing a 0.5 G margin for dispersion performance. Heat rate is constrained to 1000 W/cm<sup>2</sup> (half the limit published by Ref. 20) over an assumed one-meter-radius sphere, although in the study results, no trajectories were limited by this constraint. Some series of runs are noted as implementing a 10 km “dip constraint”, which constrain those trajectories to minimum altitudes no less than 10 km, reflecting the desire to limit the extent to which a vehicle is allowed to skim close to the ground prior to a loft to a higher altitude. Additionally, trajectories are automatically terminated if they fall below -5 km in altitude.

As summarized in Table 3, the effective matrix of runs for this study consists of inertial entry velocities of 3.3 km/s (representative of entry from a 500 km circular orbit), 4.7 km/s (representative of entry from a 1-sol elliptical orbit), and 5.5 km/s (representative of a direct entry). Note that, while entry velocities reported are inertial, they are approximately equal to the relative entry velocity since the assumed entry azimuth is 0° (north). Ballistic coefficients range from 200 to 1000 kg/m<sup>2</sup> in increments of 200 kg/m<sup>2</sup>, and lift-to-drag ratio ranges from 0.2 to 0.9 in increments of 0.1. Altitude is maximized at four distinct termination Mach numbers meant to represent potential parachute, inflatable, or propulsion deployment points: Mach 0.8, 2.0, 3.5, and 5.0.

**Table 3. Parameterization of Vehicle and Boundary Condition Variables.**

Parameter	Values Assessed
Inertial Entry Velocity (km/s)	3.3, 4.7, 5.5
Termination Mach Number	0.8, 2.0, 3.5, 5.0
Vehicle Ballistic Coefficient (kg/m <sup>2</sup> )	200, 400, 600, 800, 1000
Vehicle L/D	0.2, 0.3, 0.4, 0.5, 0.6, 0.7, 0.8, 0.9

### III. Simulation and Optimization Method

#### A. Entry Simulation

The entry simulator used in this study is selected to allow quick, accurate trajectory simulation. A custom MATLAB simulation models vehicle motion about an assumed spherical, rotating planet in a planet-centered inertial frame. Only three forces act on the vehicle: lift, drag, and gravity. These vector forces are translated into accelerations for the assumed constant-mass vehicle and integrated over time using MATLAB’s *ode45* function. No bank rate or bank acceleration limitations are modeled. Note also that, as is applicable for skip-entry cases, atmospheric density is assumed to be zero above 125 km in altitude. Planet-specific simulation constants are shown in Table 4. Sample trajectory results from the MATLAB simulation were validated against trajectories generated via the Simulation and Optimization of Rocket Trajectories (SORT) tool used extensively at NASA JSC.

**Table 4. Mars Entry Simulation Constants.**

Mars Atmospheric Constants		Mars Physical Constants	
Ratio of Specific Heats	1.289	Gravitational Parameter	42828 km <sup>3</sup> /s <sup>2</sup>
Molecular Weight	43.34 g/mol	Planetary Radius	3396 km
Specific Gas Constant	191.8 J/kg/K	Rotational Period	24.62 hours
Maximum Altitude of Atmosphere	125 km	Sphere of Influence Altitude	571140 km

#### B. Optimizer

To allow a thorough global search through the bank-angle and entry-flight-path-angle space, the optimizer selected is a particle swarm optimizer written originally for use on Mars Science Laboratory entry optimization.<sup>21</sup> MATLAB’s *fmincon* gradient optimizer was also considered but yielded suboptimal results for early test cases.

Optimizations involve 50 particles limited to 100 iterations<sup>‡</sup> to determine the maximum altitude attainable by varying the inertial entry flight path angle and 10 bank angles evenly spaced along the expected relative velocity range. Bank angles are limited to a range of 0° to 180°, and entry flight path angle is limited to skip-out and g-limited ranges computed prior to the optimization process. The entry flight path angle g-limit is defined by the

<sup>‡</sup> In some highly constrained problems in which a 10 km dip constraint is imposed, 10 particles are limited to 500 iterations in order to speed the particle swarm initialization process, which would otherwise take over a week of computer run time.

steepest entry flight path angle for which a full-lift-up bank profile does not exceed the specified deceleration limit. The skip-out limit is defined by the shallowest entry flight path angle for which a full-lift-down bank profile causes the simulation to terminate at its 7-day time limit (allowing the optimizer to consider skip-entry trajectories). Otherwise, simulations would terminate based on Mach number (0.8, 2.0, 3.5, or 5.0) or at a -5 km altitude.

## IV. Results and Discussion

The data from this study yields a wealth of information on characteristics of Mars entry physics and implications for the design of future Mars entry vehicles (crewed or otherwise). By no means is this section comprehensive in covering the implications of all this data; however, the most important trends and implications are illustrated.

Three distinct sub-studies were implemented – a baseline sub-study defined by the assumptions and constraints listed earlier in this paper and two additional sub-studies which utilized changes to those assumptions or constraints. A full-lift-up sub-study is implemented identically to the baseline except that bank angle is constrained to be  $0^\circ$  (i.e. full-lift-up) and the only free variable is entry flight path angle. The full-lift-up study demonstrates how often a full-lift-up profile can approximate an optimal bank profile. A 30-G-constrained sub-study is implemented identically to the baseline except that the 4.5-G deceleration constraint is replaced by a 30-G constraint. This deceleration constraint change is meant to provide insight into the optimal nearly-unconstrained bank angle profile and could also be applicable to unmanned vehicles which are restricted in their deceleration only by structural limitations.

### A. Baseline Sub-Study Results

Shown in Fig. 5 is a plot of the baseline sub-study results, showing the maximum attainable final altitude (the objective function of the optimization) as a function of ballistic coefficient, lift-to-drag ratio, termination Mach number, and whether the 10 km dip constraint is imposed. This figure corresponds to an entry velocity of 4.7 km/s, but it is also representative of the 3.3 km/s and 5.5 km/s plots since it is found that, if bank control is permitted, maximum altitude performance is almost independent of entry velocity. It should also be noted that, while Mach 0.8 termination cases were run, none returned any viable trajectories (i.e. trajectories which did not hit -5 km altitude prior to reaching Mach 0.8).

The first note to make about this figure is that, as would be expected, for a given termination Mach number and dip constraint, maximum attainable altitude increases with increasing lift-to-drag ratio and decreasing ballistic coefficient. There are no local extrema, meaning that from a performance perspective, high lift-to-drag ratio and low ballistic coefficient are always desirable.

Besides yielding numbers for the maximum attainable altitude, Fig. 5 can also be interpreted as showing “iso-altitude-performance” contours. For example, for Mach 5 altitude performance with no dip constraint imposed, a 200 kg/m<sup>2</sup> vehicle with  $L/D = 0.6$  is equivalent to a 600 kg/m<sup>2</sup> vehicle with  $L/D = 0.9$ . In this way, it can be seen that a ballistic coefficient decrease can be traded against a lift-to-drag ratio increase and vice-versa. This is important to note because, typically, as an entry vehicle shape is altered to improve  $L/D$ , its ballistic coefficient increases. Again, as discussed earlier, under the assumption of trimmed hypersonic flight, from the atmospheric perspective a vehicle may be completely defined by its ballistic coefficient and lift-to-drag ratio.

Another observation which can be made from Fig. 5 is that imposition of the 10 km dip constraint (shown in the plots on the right) effectively changes the concavity of the altitude contours. Vehicles of low ballistic coefficients and high lift-to-drag ratios are unaffected by the constraint (these trajectories meet the constraint even when it is not imposed on the optimization), but vehicles at high ballistic coefficients and low lift-to-drag ratios are entirely eliminated from the data set (these trajectories cannot attain final altitudes greater than 10 km even without the constraint). Vehicles between these extremes show reduced altitudes compared to those attainable without the constraint.

Finally, and perhaps most importantly, examination of the trajectories associated with each data point in Fig. 5 yields some insight into the physics of the optimal trajectories which are converged upon. Eight specific trajectories are detailed below to illustrate trends observed from the wealth of data generated from this study.

#### 1. Apollo-Class Vehicle Trajectories

The following example trajectories approximate the performance of an Apollo-class vehicle as one with a ballistic coefficient of 400 kg/m<sup>2</sup> and lift-to-drag ratio of 0.3 (Table 2 shows the actual Apollo ballistic coefficient as 380 kg/m<sup>2</sup> and lift-to-drag ratio as 0.32, although this did vary slightly from mission to mission). It can be shown that even with bank angle control, the Apollo command module would not be able to decelerate to a velocity slower than Mach 2.1 prior to reaching 0 km altitude on Mars. Examined here is the maximum altitude Apollo could reach at Mach 5 (e.g. if the vehicle were to have a supersonic decelerator to deploy at Mach 5).

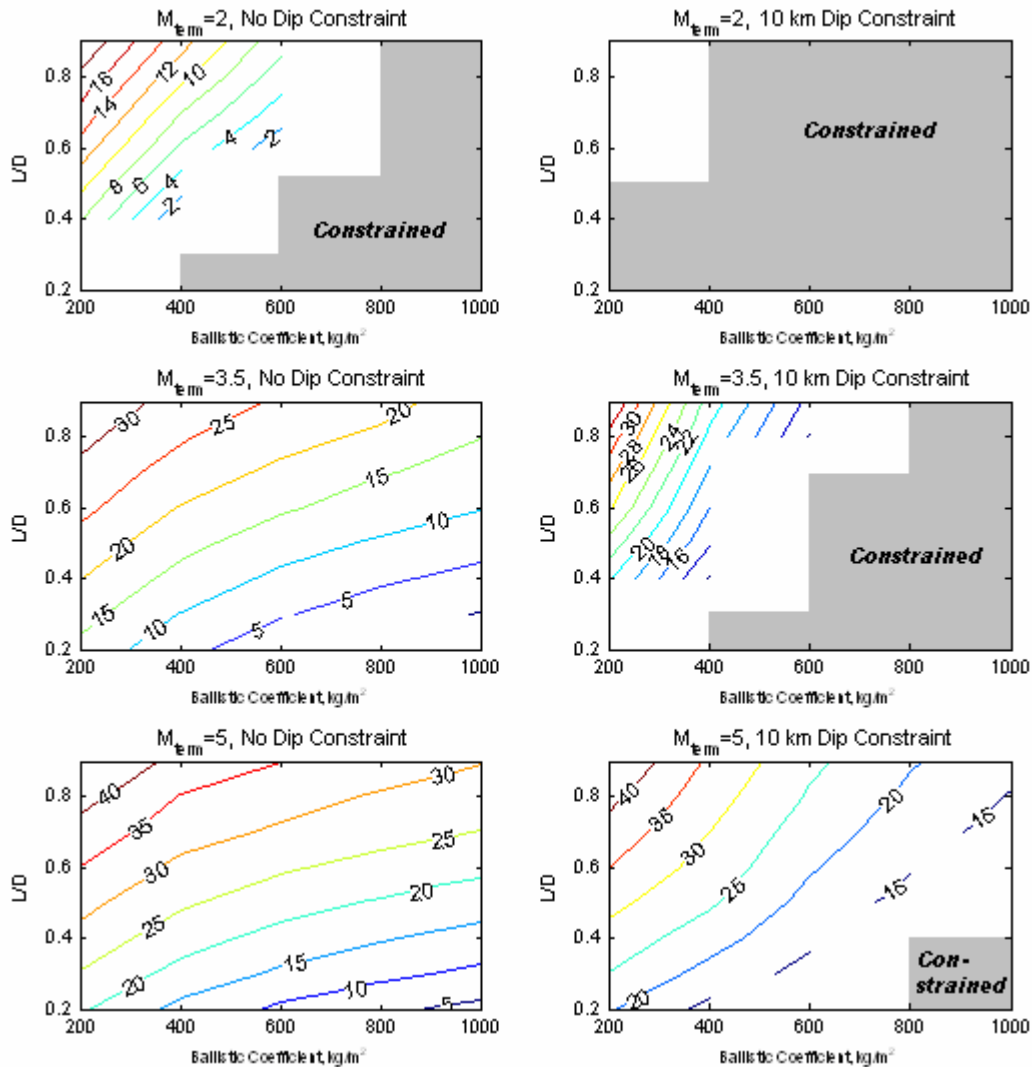


**Figure 5. Maximum attainable altitude (in km) for an entry velocity of 4.7 km/s.**

Gray regions indicate regions in which no solutions are found due to constraints. White regions with broken or absent contours indicate the boundary between the constrained and unconstrained regions.

### *Apollo-Class Entry at 4.7 km/s*

Figure 6 shows the maximum-final-altitude trajectory for an Apollo-class vehicle entering Mars' atmosphere at 4.7 km/s (e.g., entry from a 1-sol orbit). The maximum attainable altitude at Mach 5 is 18.3 km, lofted from a minimum altitude of 12.7 km (thus, this trajectory meets the 10 km dip constraint). Note that the deceleration constraint of 4.5 G's is reached and limits performance. Of particular interest is the zig-zag bank profile as the maximum deceleration point is approached, which serves to limit this maximum deceleration while still maximizing final altitude. Also note that the optimum bank profile is full-lift-up starting at approximately 3000 m/s (somewhat under Mach 15).<sup>§</sup>

<sup>§</sup> One interesting feature in virtually all of these trajectories is a peak altitude which occurs prior to the end of the trajectory (one would intuitively expect the maximum altitude for a given Mach number to occur at the top of a loft). While this feature is difficult to physically explain, it is so consistent within this study that it is believed to be a real characteristic. Independent optimization routines using the POST simulation at NASA Langley Research Center have yielded solutions with equally consistent early peaks.

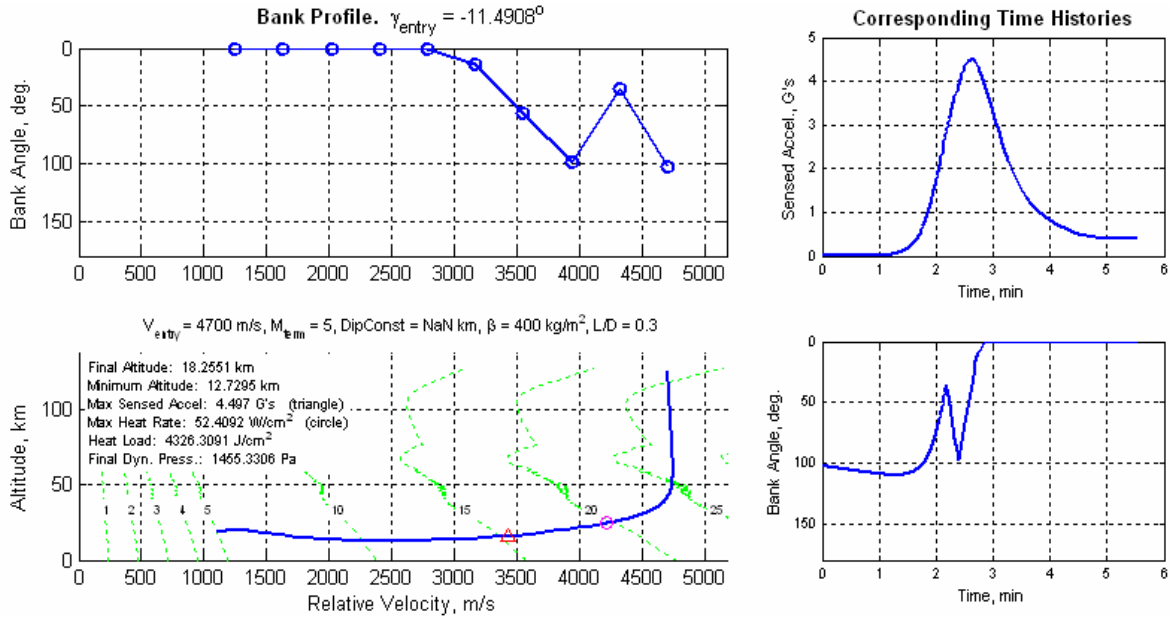


Figure 6. Optimal trajectory data for an Apollo-class vehicle entering at 4.7 km/s.

**Apollo-Class Entry at 3.3 km/s**

Figure 7 shows maximum-final-altitude trajectory data for the same vehicle entering at 3.3 km/s (e.g., entry from a low Mars orbit). The maximum attainable altitude at Mach 5 is 14.1 km, which is achieved without lofting. Note that the deceleration constraint is not approached (maximum deceleration is 1.7 G's), which is typical of low-L/D, low-entry-velocity cases in this study. Entry flight path angle is quite shallow, and the trajectory is effectively full-lift-up. Note also that the duration of the flight is about 1.5 minutes longer than the 4.7 km/s entry case.

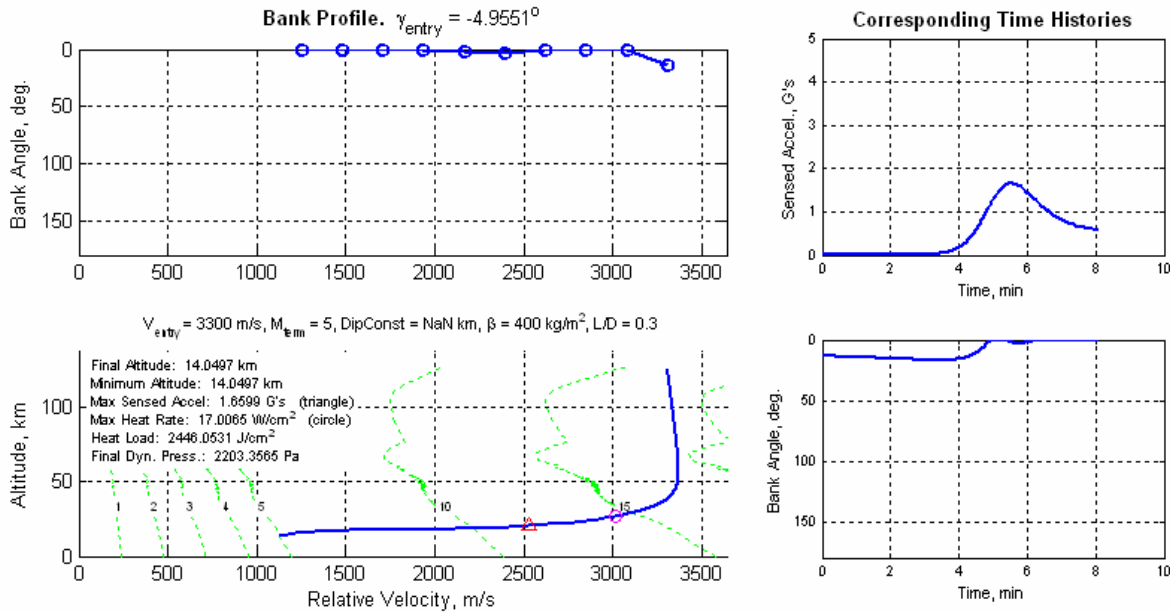


Figure 7. Optimal trajectory data for an Apollo-class vehicle entering at 3.3 km/s.

### Apollo-Class Entry at 5.5 km/s

Figure 8 below shows maximum-final-altitude trajectory data for the same Apollo-class vehicle entering at 5.5 km/s (e.g., direct entry). Similarities to the 4.7 km/s case abound. Note the similarity in maximum and minimum altitude to the 4.7 km/s case (both have a final maximum altitude of 18.3 km, and the minimum altitudes differ by only 98 m). Note also the double acceleration peak, indicating not only that the maximum allowable acceleration is a significant constraint, but also that it is a dynamic that the optimizer is attempting to follow in order to maximize altitude. The optimum entry flight path angle is within  $0.3^\circ$  of the 4.7 km/s case, and bank angle is once again  $0^\circ$  for the final 3000 m/s of the trajectory. One additional note to highlight, however, is the fact that no bank rate or acceleration limitations are assumed in these studies, and this trajectory allows bank angle to change quite rapidly from  $0^\circ$  to  $180^\circ$  in approximately 12 seconds.

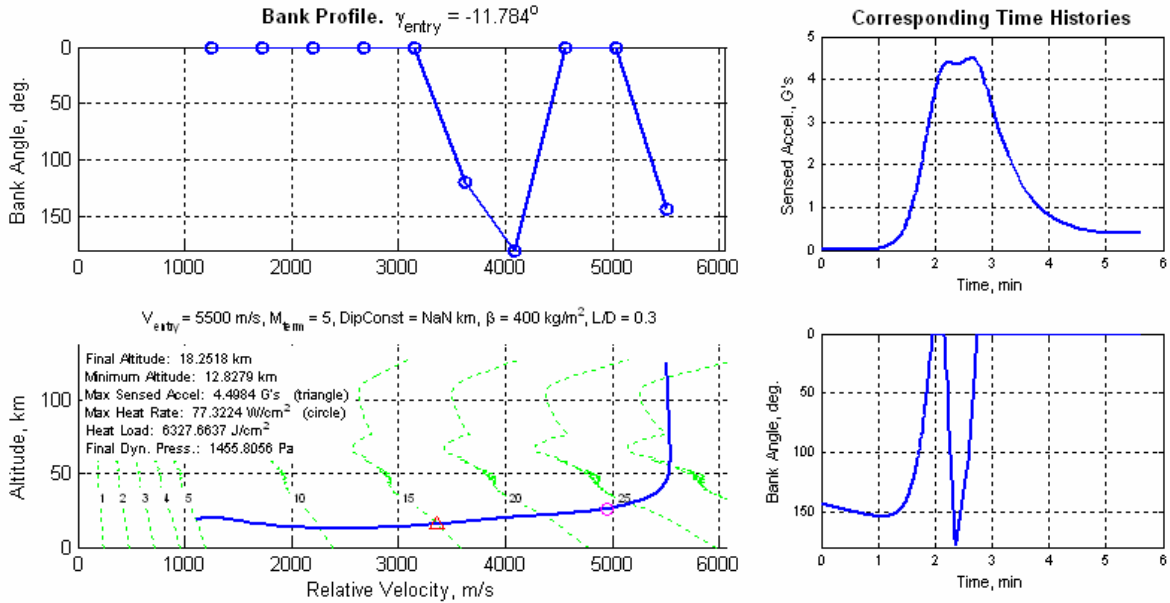


Figure 8. Optimal trajectory data for an Apollo-class vehicle entering at 5.5 km/s.

### 2. Deceleration-Limited Trajectory Illustration

The trajectory shown in Fig. 9 below illustrates the significance that the 4.5 G constraint has on limiting some of the trajectories in this study. For this high- $L/D$  ( $L/D = 0.6$ ), low-ballistic-coefficient ( $\beta = 200 \text{ kg/m}^2$ ) vehicle, three distinct deceleration peaks of nearly equal magnitude are seen in close proximity to each other, corresponding directly to the oscillation of the bank angle. This effective constant-deceleration region occurs over almost 2000 m/s of the trajectory (from approximately Mach 20 until Mach 10).

In contrast, when the 4.5-G constraint is replaced with a 30-G constraint, the optimal trajectory shown in Fig. 10 results. The differences are very pronounced. When unconstrained by deceleration limits, the deceleration load peaks at 16.2 G's. Minimum altitude drops to 5.5 km (as opposed to 12.9 km), and maximum achievable final altitude rises by 8.2 km to 34.4 km. To achieve this, entry flight path angle is steepened by  $13.5^\circ$ , giving a very steep  $-25.2^\circ$ . The trajectory is full-lift-up very early during entry, starting at approximately Mach 18. This steep-flight-path-angle, full-lift-up behavior appears to be quite typical of optimal trajectories when acceleration constraints are released.

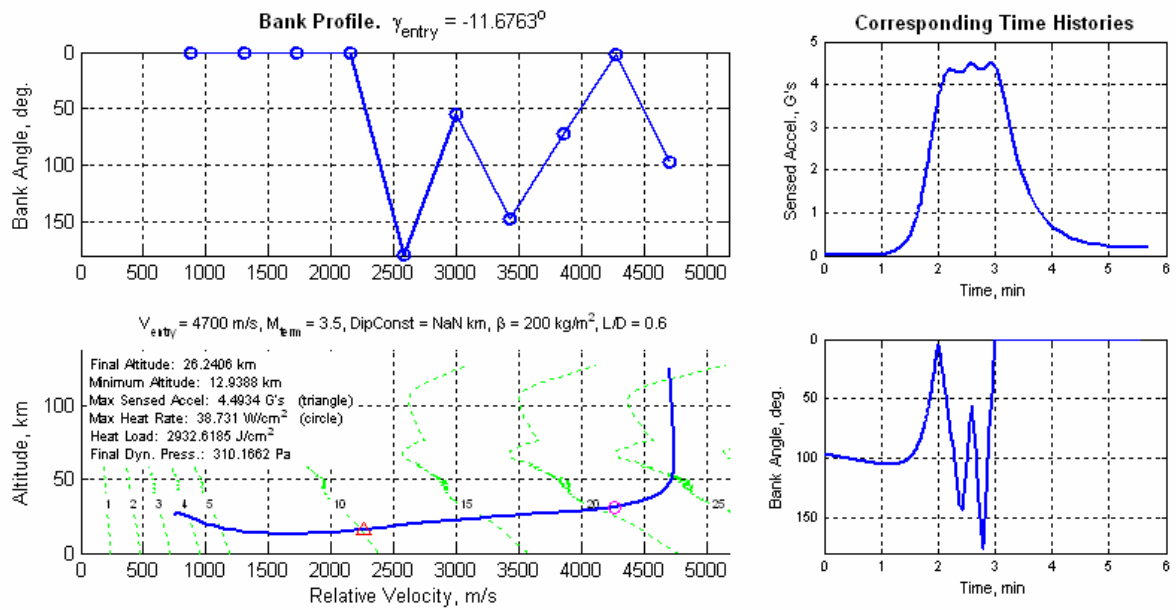


Figure 9. Optimal trajectory data for a 4.5-G constrained case.

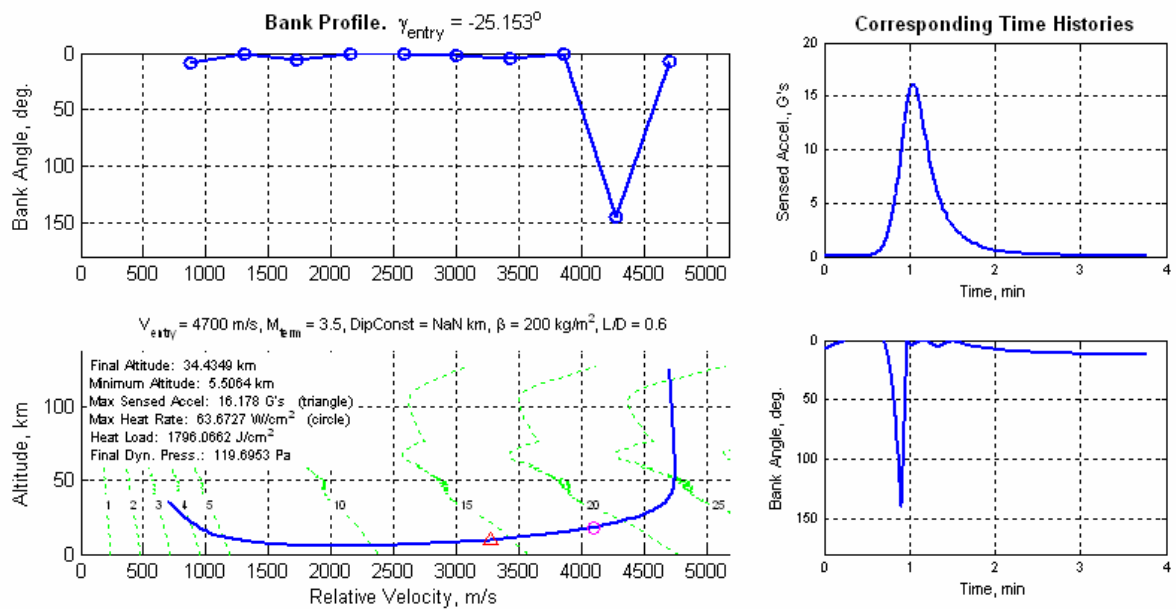
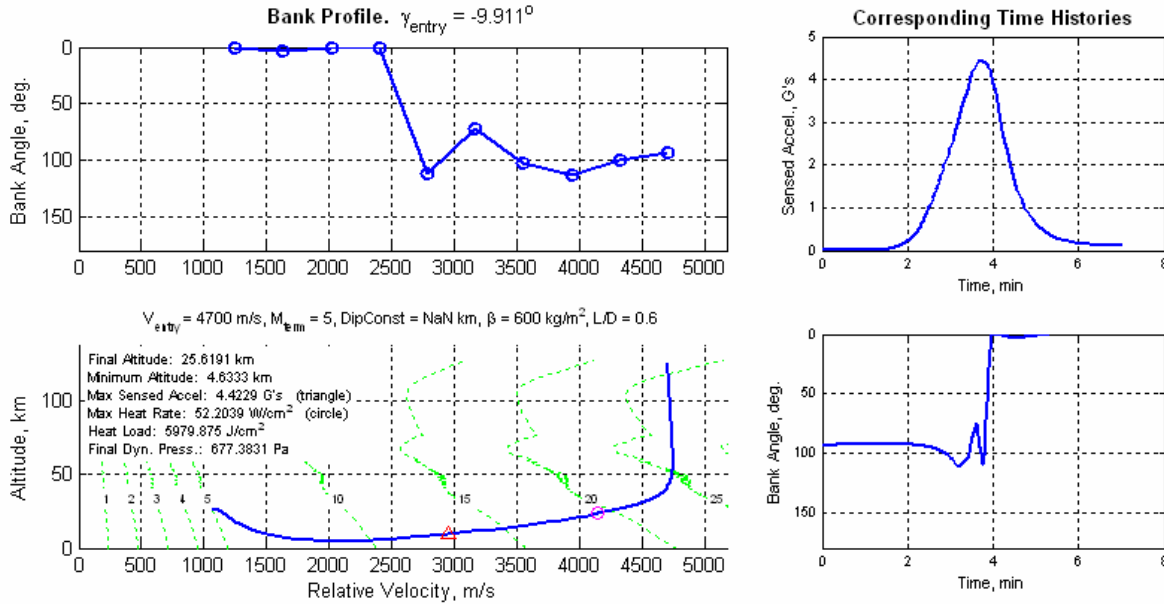


Figure 10. Optimal trajectory data for the same case as in Fig. 9 with no effective deceleration constraint.

### 3. Dip Constraint Illustration

The trajectory shown in Fig. 12 is for an identical case as the trajectory in Fig. 11 except with an added 10 km dip constraint. For this high- $L/D$  ( $L/D = 0.6$ ), moderate-ballistic-coefficient ( $\beta = 600 \text{ kg/m}^2$ ) vehicle, note that, while the nominal case dips to 4.6 km in order to reach a final altitude of 25.6 km, the case with the dip constraint dips only to 10.1 km and lofts only to 20.5 km. The dip-constrained case is also clearly not limited by acceleration (unlike the nominal case), as it only hits the 4.0-G mark. Note also the fluctuation in the dip-constrained bank profile, as opposed to the smoothness of the nominal profile.



**Figure 11.** Optimal trajectory data for a  $600 \text{ kg/m}^2$ ,  $L/D = 0.6$  vehicle.

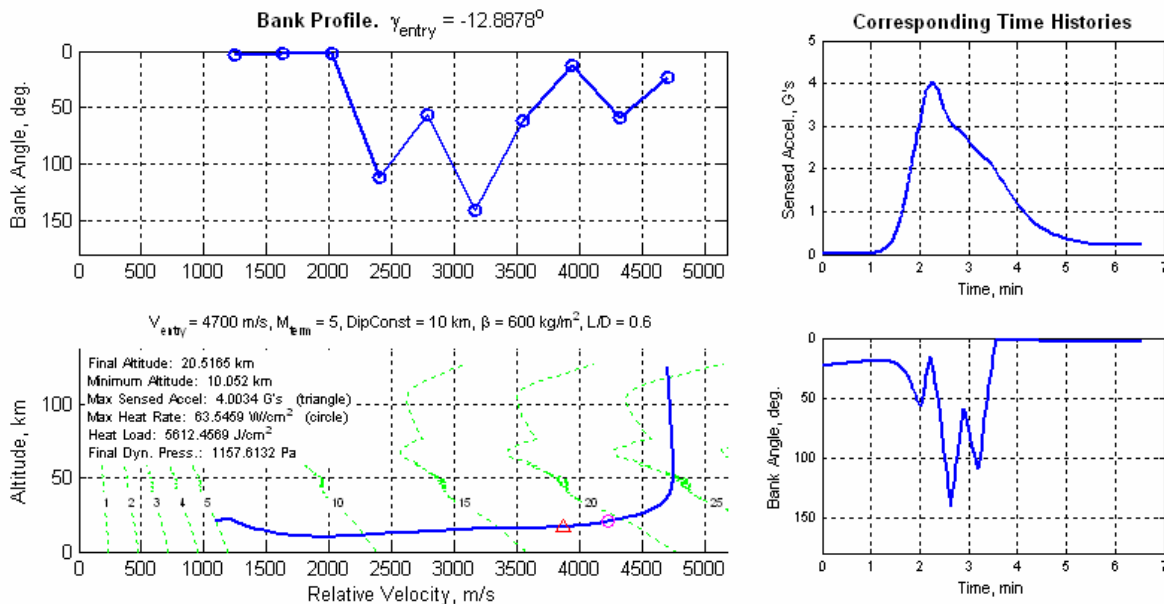


**Figure 12.** Optimal trajectory data for the same case as in Figure 11 but with a 10 km dip constraint.

#### 4. Skip-Entry Illustration

The trajectory shown in Fig. 13 is illustrative of the behavior of optimal trajectories for very-high- $L/D$  cases ( $L/D = 0.8$  or  $0.9$ ). The vast majority of these very-high- $L/D$  cases exhibit skip-entry behavior for one or several skips over a period of hours. In the case in Fig. 13, an initial skip (during which the peak heat rate is experienced) removes about 900 m/s of velocity from the vehicle with a maximum acceleration of 1.8 G's. A suborbital coast period occurs next, during which the vehicle reaches an apoapsis altitude of 1800 km (not shown) and re-enters the atmosphere at 3.8 km/s. The 4.5-G limit is hit on the second entry, and bank angle is  $0^\circ$  below about Mach 7.

The reason for this skip behavior is not entirely clear, but its consistency for nearly all very-high- $L/D$  cases makes it unlikely to be an anomaly. One reason for its optimality may be the fact that the skip(s) allow the vehicle to effectively re-enter the atmosphere at a lower velocity, which is known to reduce peak deceleration (as discussed earlier). This capability to artificially lower entry velocity through skipping may exist for lower  $L/D$  values but was not found to be optimal.

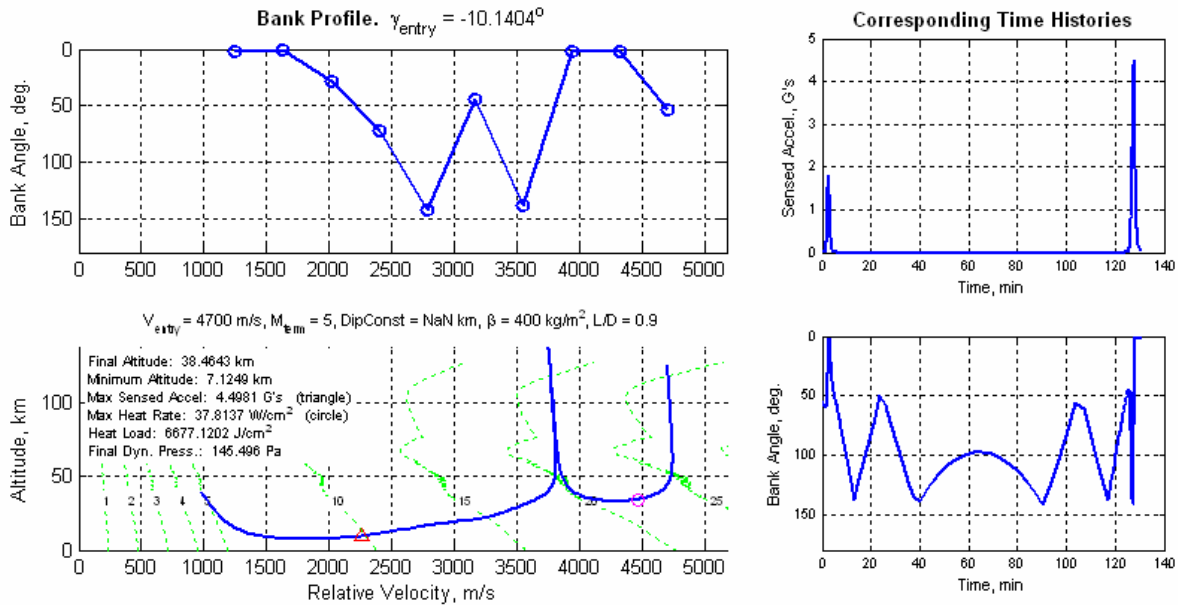
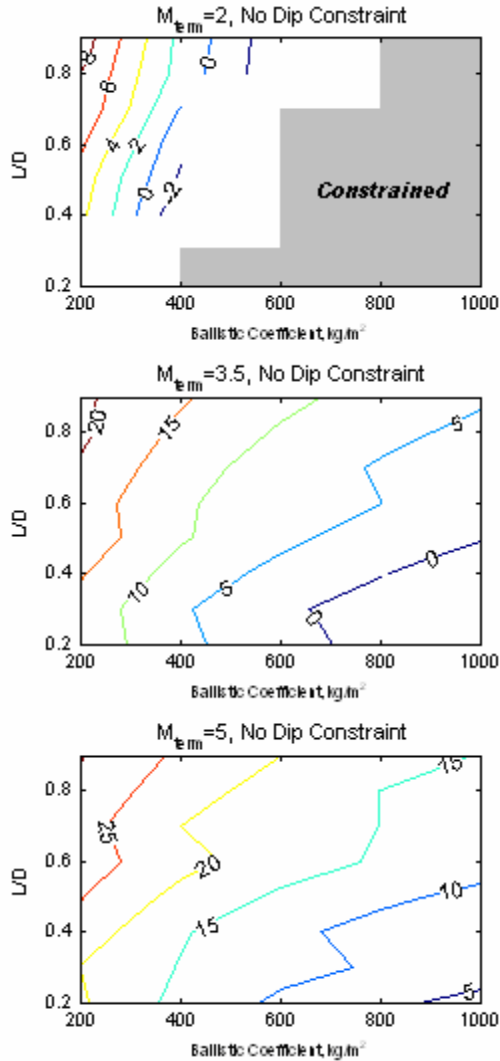


Figure 13. Optimal trajectory data for a  $400 \text{ kg/m}^2$ ,  $L/D = 0.9$  vehicle.

#### B. Full-Lift-Up Sub-Study Results

In addition to the baseline study described for the bulk of this report, a full set of optimizations (minus the 10-km dip-constrained cases) was performed for a full-lift-up profile. Thus, final altitude at all Mach numbers under consideration was maximized by varying entry flight path angle. The results of these optimizations for the 4.7 km/s entry velocity are shown in Fig. 14 in terms of maximum attainable altitude. Interestingly, zig-zag patterns exist in these contours which correlate with boundaries between skip trajectories. For example, for Mach 5 termination, optimal trajectories for vehicles with  $L/D$  values greater than about 0.3 involve a significant loft at high velocities (a “half-skip”). Then, above an  $L/D$  of about 0.7, optimal trajectories exhibit one full skip plus a significant loft (a “one-and-a-half skip”). At the  $L/D = 0.3$  and 0.7 locations, trajectories are deceleration-limited but are not deceleration-limited in the surrounding  $L/D$  regions. This behavior is consistent but so far does not have a clear physical explanation; these optimum trajectories between the deceleration-limited regions are some of the few in this study which do not appear to be limited by any one constraint.

Figure 15 shows the difference between these full-lift-up results and those of the baseline study. Note that at very low  $L/D$  values, altitudes are similar (i.e. the difference is near zero). However, as  $L/D$  increases, the benefit of bank angle control during entry becomes increasingly pronounced. Even for a low- $L/D$  vehicle such as an Apollo capsule, using a banked (instead of full-lift-up) profile could result in 4 km final altitude gains at Mach 3.5 and 5 and a 1 km final altitude gain near Mach 2. This highlights the importance of considering bank angle control in preliminary entry trajectory design.



**Figure 14.** Maximum attainable altitude (in km) for an entry velocity of 4.7 km/s under a full-lift-up bank profile.

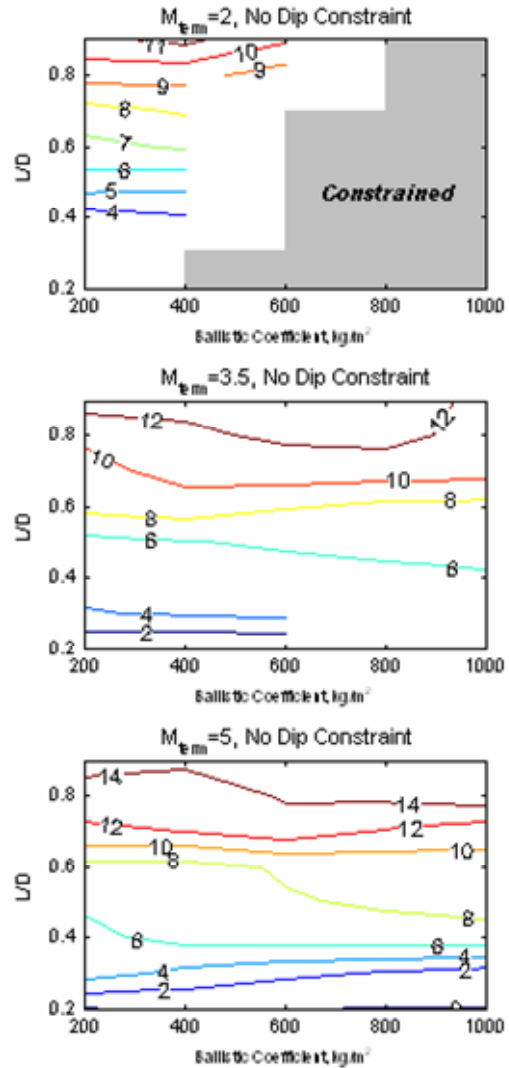


**Figure 15.** Difference in maximum attainable altitude (in km) between the baseline and full-lift-up sub-studies for a 4.7 km/s entry velocity. Note that there is clearly a greater benefit to bank angle control as L/D increases.

### C. 30-G Constrained Sub-Study Results

A third set of optimizations is performed, again to complement the baseline sub-study described for the bulk of this paper. In this third set, the 4.5 G deceleration constraint is relaxed to 30 G's, meant to effectively remove the deceleration constraint. This modification had the dual purposes of theoretically revealing “purer” optimum bank profiles which would be unconstrained by the strict 4.5-G deceleration limit and showing potential optimum trajectories for uncrewed (e.g. cargo or robotic) missions.

The maximum final altitude results from this study are shown in Fig. 16 below. Note that the altitudes seen here are, depending on the specific case, up to 16 km higher than those seen in the baseline study. Also note the interesting change in contour concavity in the high-L/D, high-ballistic-coefficient region of the Mach 3.5 and Mach 5 plots. Interestingly, analysis of the trajectories associated with this region indicates that these trajectories are actually constrained by the -5 km altitude limit within the entry simulation. Thus, this concavity change is analogous to the concavity difference between the baseline study's nominal and 10-km dip-constrained cases.

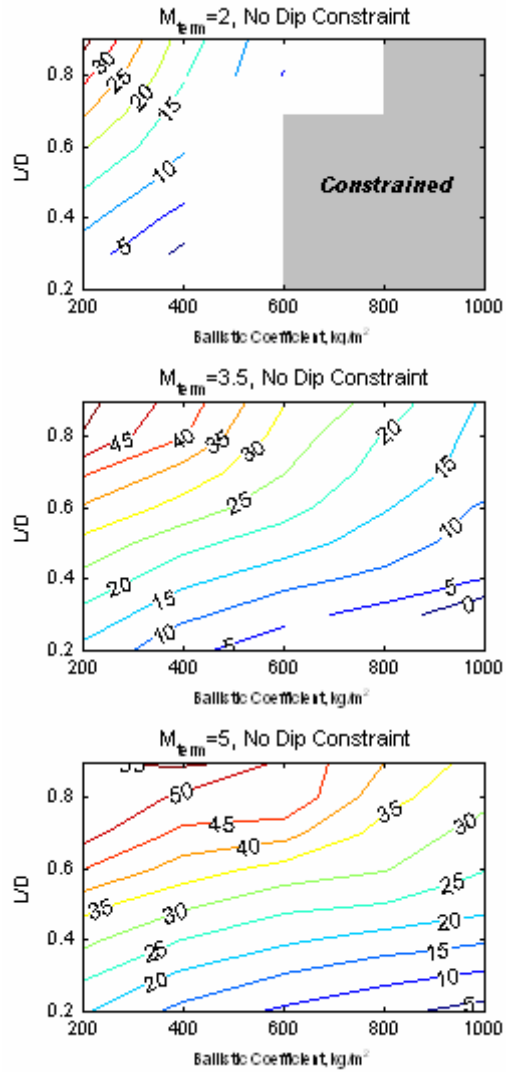


**Figure 16. Maximum attainable altitude for a 4.7 km/s entry velocity under a 30-G constraint.**  
*Note that substantially higher altitudes are achievable compared to Fig. 5.*

## V. Conclusions and Implications

This study has generated a wealth of data and insight into the characteristics of optimal trajectories for a wide range of combinations of ballistic coefficients, lift-to-drag ratios, entry velocities, termination Mach numbers, and dip constraints. In the completion of this study, more than 9 million trajectory runs were completed to optimize more than 1,800 data points. By choosing to analyze these scenarios in a vehicle-independent fashion (by assuming constant hypersonic aerodynamic coefficients), the vehicle analysis described next is made possible.

### A. Vehicle Implications

The advantage to choosing a vehicle-independent analysis is that all performance data gathered in this study is valid for any vehicle (within the bounds of uncertainty due to the constant hypersonic aerodynamic coefficients assumption). Thus, if performance of a specific vehicle is desired, only its ballistic coefficient and lift-to-drag ratio are required and its optimal altitude performance is known. Specific vehicles are points in the ballistic-coefficient vs. lift-to-drag-ratio domain. Generic vehicle shapes may be represented as contours in this domain since center of mass location and vehicle mass may vary to change both ballistic coefficient and  $L/D$ .

Figure 17 and Fig. 18 below show the Mach 3.5 and Mach 5 performance of entry vehicles entering at 4.7 km/s under a 10 km dip constraint. Overlaid on those altitude contours are iso-mass contours for three ellipsled designs plus a 12 m diameter capsule design. Additionally, Apollo and Soyuz designs are shown at their respective locations on the plots. Note that the 10 km dip constrained plot is shown because the 10 km limit is taken to represent a realistic margin above the ground to account for dispersions and safety considerations. Additionally, it should be noted that this 10 km constraint is relative to MOLA and not ground level (so the situation would be significantly more constrained if landing sites higher than 0 km MOLA are desired).

These figures illustrate several very important points about requirements for high-ballistic-coefficient Mars entry vehicle designs. First, it is clear that, when restricted to diameters below 12 m, an Apollo-class vehicle design for a high-mass crewed Mars mission is on the fringes of what is acceptable if no supplementary deceleration is available prior to Mach 3.5 (it lies very close to the gray region in which it is impossible to meet the 10 km dip constraint). For a 12 m capsule above about 100 metric tons in entry mass, deployment or activation of some decelerator device is required by Mach 5 if a 10 km dip constraint is not to be breached. Similarly, for a 12 m capsule above about 60 metric tons in entry mass, decelerator activation is required by Mach 3.5. These masses are fairly low considering the 40+ metric ton *landed* masses which are often desired for human Mars design reference missions.

For a capsule, the only way to improve this mass performance is to increase capsule diameter\*\*, which would decrease ballistic coefficient and shift the capsule contours to the left in the figures below. A capsule diameter conversion chart is shown in Table 5. Each of the brown contours in Fig. 17 and Fig. 18, which are plotted for a 12 m capsule diameter, can be re-labeled with the masses shown in Table 5 if a different capsule diameter is assumed. For example, the performance curve for a 40 t (40 metric ton) 12-m capsule is the same as for a 62.5 t, 15-m capsule.

**Table 5. Equivalent-ballistic-coefficient capsule mass conversion chart.**

10-m Capsule Mass (t)	12-m Capsule Mass (t)	15-m Capsule Mass (t)
27.8	40	62.5
41.7	60	93.8
55.6	80	125.0
69.4	100	156.3

Slender-body shapes such as ellipsleds can perhaps perform better than capsules, but they are still significantly constrained to large vehicles with relatively small payload masses. Fig. 17 shows that a  $12 \times 35$  m ellipsled allows an entry mass between 120 and 140 metric tons to reach Mach 3.5 without the assistance of a supplementary decelerator. An additional note of interest is that a given vehicle shape and mass does have its own maximum attainable altitude which can be visually found via the intersection of altitude and vehicle mass contours (for example, the maximum altitude that the 120 metric ton ellipsled described above can reach at Mach 3.5 is about 15 km, if subject to the 10 km dip constraint).

---

\*\*Unless in-space assembly is considered, a practical limit on vehicle diameter is launch vehicle fairing diameter. For example, the anticipated fairing diameter of the Ares V rocket is in the range of 8.4 m to 12 m.<sup>22</sup> In this respect, slender-body shapes such as ellipsleds offer advantages over capsules in that they can accommodate more volume (and potentially mass) for a given vehicle diameter.

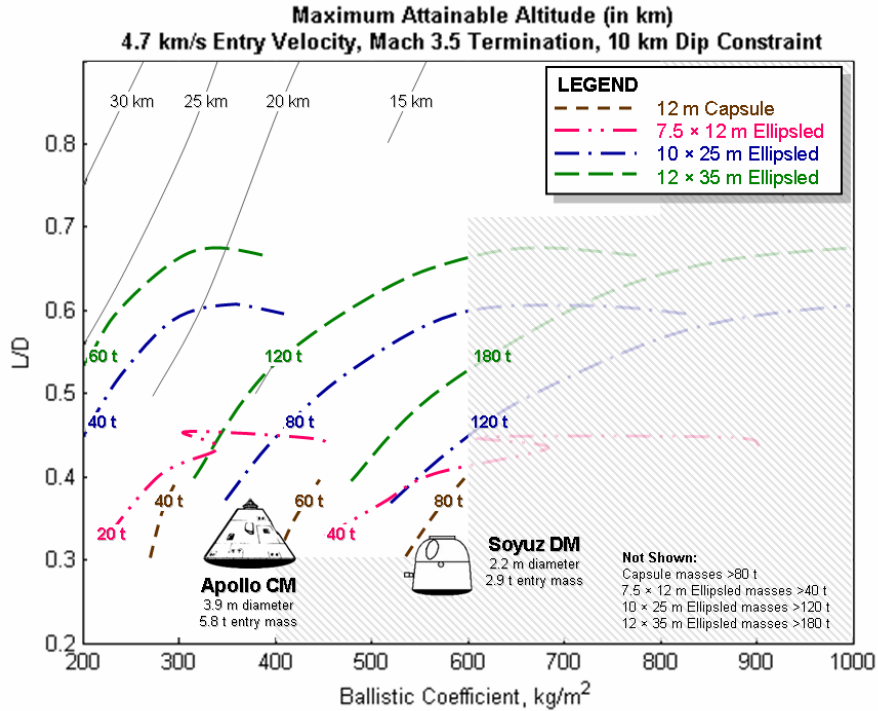


Figure 17. Overlay of Mach 3.5 maximum attainable altitude contours (shown in gray) with ellipsled and 12 m capsule vehicle characteristic contours. Note that the gray shaded region indicates the design space in which it is known that no solutions exist.

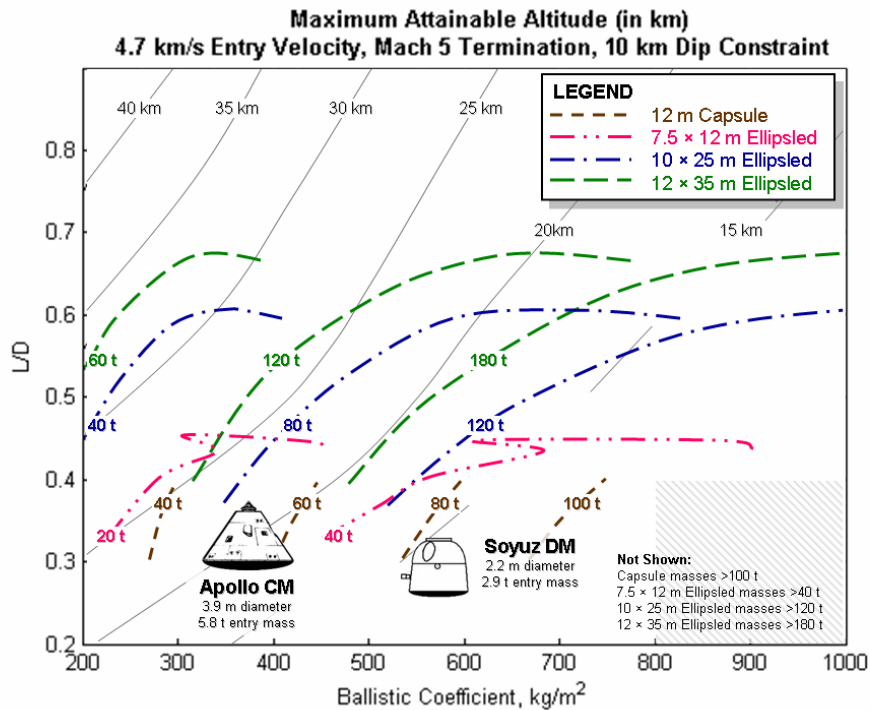


Figure 18. Overlay of Mach 5 maximum attainable altitude contours (shown in gray) with ellipsled and 12 m capsule vehicle characteristic contours. Note that the gray shaded region indicates the design space in which it is known that no solutions exist.

## B. Key Conclusions

Key conclusions from the data presented throughout this paper include:

- ***Unless vehicle  $L/D$  is low (about 0.2 or lower), entry velocity is low (under roughly 3.5-4.0 km/s), or deceleration constraints are absent or very high (in the 20's of Earth  $G$ 's), optimal banking should be considered in the preliminary design of entry trajectories.*** This study found that, for entry velocities of 4.7 km/s and 5.5 km/s, the optimal bank profiles for  $L/D = 0.2$  vehicles were primarily lift-up. For the 3.3 km/s entry velocity, optimal bank profiles for vehicles with  $L/D$  values less than 0.6 were also primarily lift-up. Additionally, for cases unconstrained by deceleration loads, the optimum-bank tendency was full-lift-up at a very steep entry flight path angle (unless altitude constraints interfered).
- ***Optimal final-altitude-maximizing bank profiles tend to be full-lift-up at the end of the trajectory, tend to have somewhat lift-down bank angles at the beginning of the trajectory, and, for higher entry velocities, almost always attempt to follow deceleration load constraints.***
- ***Multiple bank profiles may be capable of reaching the same (or nearly the same) optimum altitude.*** Contours shown in final altitude plots in this study all appear smooth, which suggests quite strongly that the true optimum altitudes were nearly always found. However, the bank angle profiles which achieve neighboring optimum altitudes often show more irregular behavior. One credible explanation of this is that multiple bank angle combinations are commonly capable of achieving the same (or nearly the same) final altitude/velocity state.
- ***Minimum altitude constraints and deceleration load constraints are significant optimal trajectory drivers.*** As shown in this study, a 10 km dip constraint can severely limit the ballistic coefficient and lift-to-drag combinations that are allowable. High- $L/D$ , low-ballistic-coefficient vehicles do not violate the constraint, while low- $L/D$ , high-ballistic-coefficient vehicles violate it simply because they cannot reach a final altitude above 10 km in the first place. Fringe cases see significant reductions when the dip constraint is imposed. Similarly, releasing a 4.5-G deceleration load constraint can result in altitude gains up to 16 km for the cases considered in this study (or approximately 2 km for an Apollo-class vehicle).
- ***Low- $L/D$  vehicle configurations (e.g. capsules and short ellipsoids) require very low ballistic coefficients to overcome their lift limitations.*** As detailed earlier, if no supplementary deceleration options (e.g., parachutes, inflatable decelerators, propulsion) are available prior to Mach 5, a 12 m diameter capsule is limited to 100 metric tons. If no options are available prior to Mach 3.5, that mass is lowered to approximately 60 metric tons. A  $12 \times 35$  m ellipsoid can reach a mass of between 120 and 140 metric tons and still reach Mach 3.5 without the assistance of a supplementary decelerator. Without decelerator assistance, Mach 2 is unachievable for  $L/D$  values of 0.5 or less (unless ballistic coefficient is less than 200 kg/m<sup>2</sup>), and Mach 0.8 cannot be achieved for any ballistic coefficient and  $L/D$  combination considered in this study.

## C. Study Limitations

This study has attempted to be as broadly applicable within the limits of time and the scope of work for the NASA Mars DRM 5.0 effort. Two principal limitations are recognized, and avenues for future follow-on work are identified.

First, this study has not considered environment and state knowledge dispersions which are crucial to any real, guided landing on Mars, especially human missions. This study has also not specified what type of guidance would be required to adequately fly the optimal trajectories which have been identified. It should be noted, however, that margin is included in these trajectories in the form of a 10 km dip constraint and a 4.5-G (instead of 5-G) deceleration limit. This study was principally concerned with maximizing altitude and assumes that adequate margin was given at this stage of design. It is hoped that this work will continue in the future and include consideration of guidance performance. One such follow-on study is documented in Ref. 23.

Second, some of the optimum low- $L/D$  trajectories for the 3.3 km/s entry velocity converged to very shallow (sometimes 0°) entry flight path angles. The reason for this is that 3.3 km/s at a 0° flight path angle is below orbital velocity at the 125 km entry interface point (meaning that, while this is still a valid elliptical orbit, the periapsis of this orbit is within the atmosphere or planet). However, this limitation is difficult to remedy without assuming an initial orbit (which would disrupt the generality of this study). Before using any of the low- $L/D$  results for the 3.3 km/s entry velocity cases, the user should check the optimized entry flight path angle to be sure that entry state can be reached from the user's initial orbit.

One concern which is acknowledged is the inherent limitation of the optimizer and bank profiles used. The smoothness of the objective function (final altitude) curves in all plots suggests that true optima were consistently found. However, the bank profile was inherently limited by the ten evenly-spaced points prescribed in the relative velocity domain. For example, it was often clear that the optimizer was attempting to follow a constant-deceleration profile, but the placement of the bank points did not allow a high degree of control over this. While the approach used in this study was suitable for the goal of a broad parametric sweep, higher-fidelity studies in the future should assess different methods of defining a bank profile which are more flexible and adaptable to recognized trends than the method used here.

Finally, in the context of winged vehicles, this study is limited in the scope of  $L/D$  values considered. As noted in Table 2, the hypersonic  $L/D$  of the Space Shuttle is 1.4, which is well outside the  $L/D = 0.9$  upper limit considered in this study's parametric sweep. Since altitude performance increases with increasing  $L/D$ , it is recognized that with a high enough  $L/D$ , it may be possible to reach the elusive Mach 0.8 termination at a reasonable altitude and avoid many of the technology hurdles involved in designing large supersonic parachutes, supersonic propulsion, or inflatable aerodynamic decelerators.<sup>††</sup> This study is unable to identify what  $L/D$  values are required to accomplish such low-Mach termination states, but this may be worthy of consideration in future studies.

Overall, this study has accomplished its original goal of determining, to a reasonable certainty, optimal bank profiles for a wide range of human-class Mars entry scenarios. It has identified both the best-case altitudes and the bank profile characteristics which generally allow those altitudes to be achieved. It is hoped that this study's result and methods will find broad use within the Mars entry community.

### Acknowledgments

The authors would like to thank the Mars DRM 5.0 Aerocapture, Entry, Descent, and Landing team led by Walt Englund and Rob Manning. Thanks are especially due to Carlos Westhelle, Lee Bryant, and Michael Grant at NASA JSC for their support throughout this study, and to Dr. Robert Braun at Georgia Tech for his inputs in the documentation phase of this project.

### References

- <sup>1</sup>Mendeck, G.F. and Carman, G.L. "Guidance Design for Mars Smart Landers Using The Entry Terminal Point Controller." AIAA 2002-4502. AIAA Atmospheric Flight Mechanics Conference and Exhibit, Monterey, 5-8 Aug. 2002.
- <sup>2</sup>Christian, J., Wells, G., Lafleur, J., et. al. "Sizing of an Entry, Descent, and Landing System for Human Mars Exploration." AIAA 2006-7427. Space 2006, San Jose, 19-21 Sept. 2006.
- <sup>3</sup>Wells, G. and Braun, R. "An Entry Handbook for the Conceptual Design of Mars Missions." AA2006-1-34. 1<sup>st</sup> International ARA Days, Arcachon, 3-5 July 2006.
- <sup>4</sup>Cruz, J.R., Cianciolo, A.D., Powell, R.W., et. al. "Entry, Descent, and Landing Technology Concept Trade Study for Increasing Payload Mass to the Surface of Mars." International Symposium on Atmospheric Reentry Vehicles and Systems Paper. Arcachon, 21-23 March 2005.
- <sup>5</sup>Lafleur, J. "Derivation and Application of a Method for First-Order Estimation of Planetary Aerial Vehicle Power Requirements." International Planetary Probe Workshop Paper. Pasadena, 27-30 June 2006.
- <sup>6</sup>Palmer, M.J. "Affordable Air – Vertical Wind Tunnel for Indoor Skydiving." AIAA 2000-0289. Aerospace Sciences Meeting and Exhibit, Reno, 10-13 Jan. 2000.
- <sup>7</sup>Braun, R.D. and Manning, R.M., "Mars Exploration Entry, Descent and Landing Challenges," IEEEAC Paper #0076, Big Sky, 4-11 March 2006.
- <sup>8</sup>Braun, R.D., Mitcheltree, R.A., and Cheatwood, F. M., "Mars Microprobe Entry-to-Impact Analysis." *Journal of Spacecraft and Rockets*, Vol. 36, No. 3, May-June 1999, pp. 412-420.
- <sup>9</sup>Stride, Scot. "Mars Micro rover Telecom Closing Comments." *Mars Microrover Telecommunications* [online]. 3 Oct. 1997. URL: <http://mpfwww.jpl.nasa.gov/MPF/rovercom/closing.html> [cited 22 July 2007].
- <sup>10</sup>Liever, P.A., Habchi, S.D., Burnell, S.I., and Lingard, J.S. "Computational Fluid Dynamics Prediction of the Beagle 2 Aerodynamic Database." *Journal of Spacecraft and Rockets*, Vol. 40, No. 5, Sept.-Oct. 2003, pp. 632-638.
- <sup>11</sup>Beagle 2 Team. "Beagle 2 System Overview." *Beagle 2* [online]. 26 Aug. 2004. URL: <http://www.beagle2.com/technology/overview.htm> [cited 22 July 2007].
- <sup>12</sup>Erb, R.B. and Jacobs, S. "Entry Performance of the Mercury Spacecraft Heat Shield." NASA-TM-X-57097. Hampton, 12-14 Oct. 1964.
- <sup>13</sup>Stewart, J.D. and Greenshields, D.H. "Entry Vehicles for Space Programs." *Journal of Spacecraft and Rockets*, Vol. 6, No. 10, Oct. 1969, pp. 1089-1102.

---

<sup>††</sup> It deserves note that other hurdles may arise due to the poorer packaging efficiency and more demanding thermal protection requirements for winged vehicles, which is a trade that must be considered at the system level.

<sup>14</sup>Johnson, N.L., *Handbook of Soviet Manned Space Flight*, AAS Science and Technology Series, Vol. 48, Univelt, San Diego, 1980.

<sup>15</sup>Whitnah, A.M. and Howes, D.B. "Summary Analysis of the Gemini Entry Aerodynamics." NASA-TM-X-58100. Nov. 1972.

<sup>16</sup>NASA Goddard Space Flight Center, National Space Science Data Center Spacecraft Query [online database], URL: <http://nssdc.gsfc.nasa.gov/database/sc-query.html> [cited 25 July 2007].

<sup>17</sup>Griffith, B.J. and Boylan, D.E. "Postflight Apollo Command Module Aerodynamic Simulation Tests." *Journal of Spacecraft and Rockets*, Vol. 5, No. 7, July 1968. pp. 843-848.

<sup>18</sup>Graves, C.A. and Harpold, J.C. "Re-entry Targeting Philosophy and Flight Results from Apollo 10 and 11." AIAA 1970-0028. Aerospace Sciences Meeting, New York, 19-21 Jan. 1970.

<sup>19</sup>Justus, C.G. and Johnson, D.L. "Mars Global Reference Atmospheric Model 2001 Version (Mars-GRAM 2001): Users Guide." NASA-TM-2001-210961. April 2001.

<sup>20</sup>National Aeronautics and Space Administration. "NASA's Exploration Systems Architecture Study." NASA-TM-2005-214062. Nov. 2005.

<sup>21</sup>Grant, M. and Mendeck, G. "Mars Science Laboratory Entry Optimization Using Particle Swarm Methodology." AIAA 2007-6393. AIAA Atmospheric Flight Mechanics Conference and Exhibit, Hilton Head, 20-23 Aug. 2007.

<sup>22</sup>Lillie, C.F., Dailey, D., Kroening, K., and Polidan, R.S. "Large Aperture Telescopes Enabled by the Ares V Launch Vehicle." AIAA 2007-6124. AIAA Space 2007 Conference and Exposition, Long Beach, 18-20 Sept. 2007.

<sup>23</sup>García-Llama, E. "Apollo-Derived Terminal Control for Bank-Modulated Mars Entries with Altitude Maximization." AIAA 2008-6819. AIAA Guidance, Navigation, and Control Conference and Exhibit, Honolulu, 18-21 Aug. 2008.